Investigation of the interaction potential between a neutral molecule and a conducting surface*

A. Shih,† D. Raskin,‡ and P. Kusch§
Columbia Radiation Laboratory, Department of Physics, Columbia University, New York, New York 10027
(Received 18 July 1973)

The interaction potential between a neutral molecule and a conducting surface is investigated through the study of the deflection of a beam of molecules by the conducting surface. The ultrahigh-vacuum system gave a vacuum below 5×10^{-11} Torr, where the scattering by the residual gas is negligible in the deflection region of interest. An r^{-3} potential is predicted from a model in which the permanent dipole of the molecule interacts with its image in the surface of an ideal conductor. The measured deflection by the conducting surface does not agree precisely in form with this predicted potential. When this small difference in form is ignored, the observed interaction constants indicate that the model does, in fact, account for the major part of the interaction. These observed constants are from 0.42 to 0.68 of the predicted values. There remain unevaluated corrections arising from the finite resistivity of the conductor, and from a contribution by the fluctuation of the instantaneous dipole moment of the molecule from its statistical average (i.e., the permanent dipole moment).

INTRODUCTION

The interaction with a conducting surface of a molecule characterized by an electric dipole moment is studied in this experiment. A simple classical picture for such a system is the dipole and image-dipole model in which the surface is assumed to be an ideal conductor.

A dipole $\vec{P}$ with coordinates $(0,0,R)$, in the presence of a conducting wall occupying the negative z half-space, induces an image dipole $\vec{P}'$ at $(0,0,-R)$; $\vec{P}'$ is related to $\vec{P}$ by $P'_x=-P_x$, $P'_y=-P_y$, and $P'_z=P_z$. Thus, the interaction energy is

$$\tilde{V}(R)=\frac{1}{2(2R)^3}[\vec{P}\cdot\vec{P}'-3(\vec{P}\cdot\hat{n})(\vec{P}'\cdot\hat{n})]$$

$$=-\frac{P^2}{16R^3}(1+\cos^2\theta), \tag{1}$$

where $\cos\theta=P_z/P$.

When a molecule in the rotational quantum state (J,M) is characterized by the dipole moment $\vec{P}$, the interaction energy is

$$\langle JM|\tilde{V}(R)|JM\rangle=-\frac{P^2}{16R^3}\left(\frac{4}{3}+\frac{2}{3}\,\frac{J(J+1)-3M^2}{(2J-1)(2J+3)}\right). \tag{2}$$

Since no selection of (J,M) states can be made in the present experiment, we are concerned only with the average interaction energy

$$V(R)=\frac{1}{2J+1}\sum_{M=-J}^{J}\langle JM|\tilde{V}(R)|JM\rangle=-\frac{P^2}{12R^3}. \tag{3}$$

We have ascribed a permanent dipole moment to a molecule. In fact, the instantaneous dipole moment of a molecule fluctuates from its statistical average, that is, the permanent dipole moment.

The interaction energy of an atom with an ideal conductor is derived by Lennard-Jones[1] by considering the interaction of the instantaneous dipole moment of the atom with its image. The same treatment is applied to a rotating diatomic molecule interacting with an ideal conductor. The energy averaged over the rotational states of the molecule is found[2] to be

$$V_{L-J}=-\frac{P^2}{12R^3}-\frac{e^2}{12R^3}\left[\langle 1\sigma|\left(\sum_i(\vec{r}_i)_x\right)^2+\left(\sum_i(\vec{r}_i)_y\right)^2|1\sigma\rangle+\sum_{K\neq 1\sigma}\left|\langle 1\sigma|\sum_i(\vec{r}_i)_z|K\rangle\right|^2\right], \tag{4}$$

with the diatomic molecule at its ground state 1σ, and where $\vec{r}_i$ is the coordinate of ith electron in the center of mass coordinates of the molecule, and the Z axis is along the internuclear line.

The interaction energies predicted by both models can be written in the form, for convenience of discussion, $V(R)=-K/R^3$, where K is referred to as the interaction constant.

While the interaction constant by Lennard-Jones model is difficult to evaluate without the wave function of the molecule, the upper limit derived from this model is clearly the interaction constant by the dipole and image-dipole model since the terms inside the large square brackets in Eq. (4) are

intrinsically positive.

In principle the difference between the observed K and the classically predicted K gives a measure of the effect of the second term in Eq. (4). In fact, even the classically predicted K is imprecise since the permanent dipole moment of the molecule is not known for all the ν, J states under observation in the present experiments. In addition, other effects as described below modify the interaction energy.

Bardeen[3] and Mavroyannis[4] considered the finite conductivity of the metal, and the derived interaction energies also have the inverse cube form. The predicted interaction constants are smaller than for the Lennard-Jones model. We are unable to evaluate the correction arising from the finite resistivity of the conductor using either Bardeen's or Mavroyannis's theory because of the complexity of the conducting materials (stainless steel and electroless nickel) used in the experiment.

Casimir and Polder[5] have studied the effect of electromagnetic retardation on the interaction potential between an atom and a conductor. When the separation R is large compared with the wavelength λ associated with transition between the ground state and the excited states of the atom, the interaction potential is found to be an R^{-4} potential.

For a polar molecule rotating about an axis perpendicular to the internuclear line and at a distance from the surface that is small compared to the wavelength associated with rotational frequency, the retardation effect is not important.

For those molecules deflected into the angles of deflection observed in the experiment, that is, between 0.1 mrad and 2.8 mrad, the impact parameters of the molecules are typically between 800 Å and 350 Å.

At 830 °K, the temperature of the oven from which the beam effuses, the most probable rotational frequency for CsCl is 2.8×10^{11} sec^{-1}, and the associated wavelength is 0.11 cm, which is much larger than the distance between molecules and the surface.

The molecular beam deflection method was first used by Raskin and Kusch[6] to investigate the interaction between an atom or a molecule with a conducting surface. In that experiment, it is found that K (CsCl on gold) = 30 D^2 (1 D = 10^{-18} esu) and K (CsCl on glass) = 10 D^2. In this work K (CsCl on stainless steel) is in the range 5.2–6.3 D^2 and K (CsCl on Ni) in the range 3.8–4.6 D^2. The discrepancy seems to be improbably large even after allowing for the "odd" properties of stainless steel and electroless nickel. We believe the present result to be more reliable. In the previous experiment, the intensity of the beam deflected into some angle due to the interaction under study was extrapolated from a large total intensity. The larger part of this intensity at a typical deflection angle, occurred through small angle scattering of the beam by the residual gas in the apparatus. In the present work, the density of the residual gas has been reduced by several orders of magnitude and no significant scattering effects occur.

Recently, Lando and Slutsky[7] have investigated the force between molecules and a conducting surface through the study of the adsorption isotherm of the molecules on the surface. Their result indicates an interaction potential of an r^{-2} form. The data of the present experiment are inconsistent with such a potential.

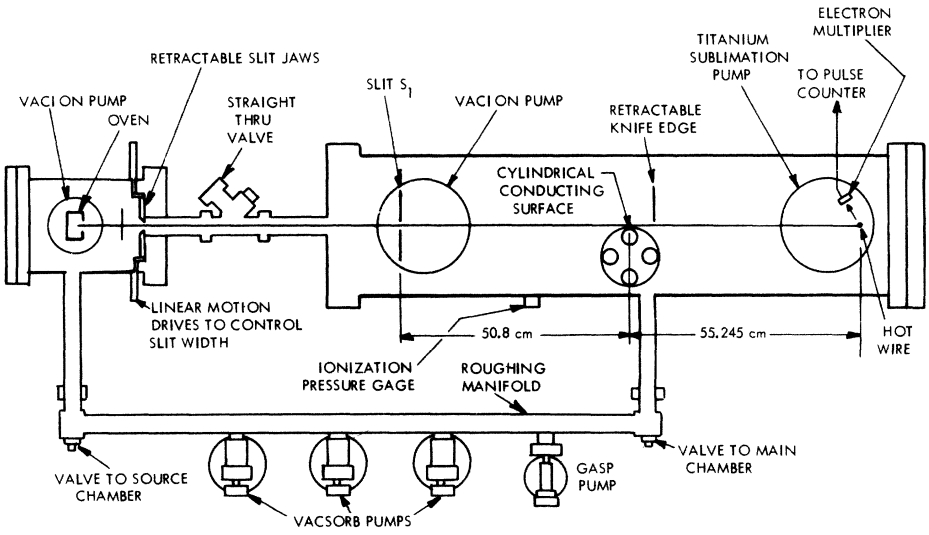

FIG. 1. Experimental apparatus.

APPARATUS

The apparatus (Fig. 1) is housed in an ultrahigh-vacuum system which consists of two separate chambers, a source chamber and a main chamber. All flanges of the system are sealed with copper gaskets, so that the entire system may be baked. The two chambers communicate only through a tube 1.5-in. in diameter and 14-in. long with a straight-through valve in the middle. The valve remains closed during the pump down, and is opened only when measurements are made.

Both chambers are pumped from atmospheric pressure to 10^{-2} Torr, first by an aspirator pump and then by sorption pumps. When the pressure falls below 10^{-2} Torr, the ion pumps are turned on and valves connecting the chambers and the roughing manifold are closed off. Therefore, the roughing process as well as the subsequent pumping avoids oil contamination of the apparatus. The main chamber is furnished with a Varian 500-l/sec vacion and a 6-in.-diam titanium sublimation pump. The source chamber is serviced by a 145-l/sec vacion pump.

The system is baked to 200 °C for 24 h. The pressure of the main chamber falls below 1×10^{-10} Torr after 48 h. For conditions under which data are taken (interchamber valve open, source oven hot, detecting filament on, etc.) the pressure in the main chamber is normally below 5×10^{-11} Torr.

In the earlier experiment,[6] there was observable scattering of the beam by residual gas in the vacuum chamber. For the experiments reported here with the background pressure below 5×10^{-11} Torr, the effect due to scattering by the residual gas is insignificant in the deflection angles of interest. If a knife edge is inserted close to the surface under study, the scattering volume, and thus the intensity due to scattering, is reduced.[6] The measured intensities at all deflection angles of interest are independent of the knife edge position.

Neutral molecules are detected by a hot tungsten wire, where, for example, cesium halides dissociate and surface ionize. The ions are field accelerated to the cathode of a Bendix magnetic electron multiplier (model 310B). The pulses from the secondary electron cascade are counted through the conventional pulse counting techniques.

Pulse rates vary from 4×10^{5} counts/sec at the full beam intensity to as low as 0.4 counts/sec for the deflected beam intensity.

While calculation indicates that 1.7×10^{7} particles/sec should arrive at the detector wire at the full beam intensity region, the number pulses counted is only about 4×10^{5} particles/sec in that region. Thus, only a very small fraction (approximately 2%) of the particles incident on the wire gives rise to observed pulses.

The poor efficiency can be explained by the small probability that a pulse is generated in the electron multiplier by an incident ion. The kinetic energy of a Cs^{+} ion that hits the nichrome cathode surface is 1500 eV. The chance of producing secondary electrons by ions of such low energy is generally small. For example, the probability of electron emission on a clean tungsten surface was found[8] to be 1.2% for a Cs^{+} ion at 1500 eV, and the adsorption of a monolayer of either O_2 or N_2 on the surface increases the efficiency by a factor of 2 or 3. In spite of the low over-all detection efficiency, we adopted the present method of detection because it allows a virtually unlimited time of observation for the very small currents that are to be measured.

A low-noise detection system is required in the measurement of the very small deflected beam intensity. The presence of potassium within ordinary tungsten wire causes large background noise. However, Frazer *et al.*[9] have developed a treatment process for tungsten wire that reduces the noise to an exceedingly low level. In this method, a commercial tungsten wire is heated in $W(CO)_6$ vapor. When $W(CO)_6$ strikes the hot wire, the reaction $W(CO)_6 \rightarrow W + 6CO$, takes place and tungsten is deposited on the wire surface while CO gas is released. We use this process to coat pure W onto a 0.0013-cm W wire until its final diameter is about 0.0022 cm. The total background noise for a wire prepared in this way is normally 0.02–0.07 counts/sec, which is small compared to the smallest ion flux involved (0.4 counts/sec). The background noise is measured with the beam shutter closed and other conditions unchanged, and its value subtracted from the total observed intensity to give the deflected beam intensity.

Five cylindrical surfaces have been used in the experiment. Three of the surfaces are 440 C stainless, two 1-in. diam and one 4-in. diam. The other two are electroless nickel cylinders 1-in. in diameter. The composition of stainless 440 C is, by weight, 1% C, 17% Cr, trace amounts of Mo, Mn, S, Si, and the rest is Fe (minimum 79%), while the electroless nickel surface is a 0.002 in. or 5000-Å thick coating of Ni with a 7–8% P, by weight, uniformly distributed. The resistivity is 60 $\mu\Omega$ cm for either stainless steel 440 C or electroless nickel.

The odd materials of the cylinders were chosen because there were minimal technical difficulties in the production of the smooth cylindrical surfaces. These surfaces, made by Speedring Corp., are polished to $\frac{1}{20}$ wavelength (~250 Å), as verified by multiple beam interferometry (performed

by Testex, Inc.). Thus, the root mean-square deviation from an ideal cylindrical surface is 125 Å, which is still significant compared to the typical impact parameters (between 350 Å and 800 Å). The detailed topography of a surface is extremely complicated; the irregularities vary in height and width as well as shape. We have no knowledge on the detailed topography of our surfaces and no workable model has been devised to study the effect of the surface roughness. However, our data suggest that this is clearly not a major effect. Four different locations on a 5-cm radius stainless-steel surface yield essentially the same beam profile.

METHOD

In the experiment a cylindrical surface partially intercepts a molecular beam emitted from a conventional oven. The beam is defined by a very narrow slit S_1, of width 10 μ (see Fig. 1). The intensity distribution of the beam is measured as a function of distance into the geometric shadow of the surface, and this intensity distribution is referred to as the beam profile.

Essential to an ideal experiment is the determination of the coordinate S_0, the position of that portion of the beam that issues from or is defined by an infinitesimal slit and is tangent to the cylindrical surface, in the absence of the interaction under study. In the ideal case, a sharp discontinuity in intensity from full intensity to zero would occur at S_0. In practice, the defining slit has a finite width, in our case 10 μ. For a detector of infinitesimal width, and in the absence of the interaction, the intensity drops linearly from its full value to zero in a distance of 10 μ, since the cylindrical surface is midway between the defining slit S_1 and the detector. It is not, of course, possible to eliminate the interaction. Hence, the intensity will drop off before S_0, but will be greater than that anticipated from a finite slit within the geometrical shadow. These two effects are inherent in determining the beam profile near S_0.

It is not possible to make all nominally parallel elements (S_1, cylinder axis, detector) precisely parallel. A significant effect of nonparallelism would be equivalent to an increased width of S_1.

Finally, it is not possible to measure the actual beam intensity with a detector of infinitesimal area. Accordingly, a detector will measure the integrated intensity over a finite width of the beam.

A typical measured intensity drop near S_0 is shown in Fig. 2. In practice, the position of zero deflection is taken to be that position at which the intensity is one-half the full value. Essentially this ignores the interaction under study. The beam profiles are measured with the detector at the distances between 0.005 cm and 0.14 cm from S_0.

A detector of a width $2W = 22$ μ is used to measure the beam intensity. The actual intensity distribution is a linear slope which drops from its full value to zero in a distance $2A$ in the absence of interaction. The shape of the intensity distribution shown in Fig. 2 is best reproduced with the value of $2A$ being 14 μ. The actual fact is that the number of particles deflected through a significant angle on the scale of these experiments is extremely small and for the purpose of finding S_0 the midpoint between full intensity and zero intensity (on scale of I_0) is extremely good.

The theoretical beam intensity $I(S)$ as given in Eq. (21) is calculated for an ideal experiment (i.e., $2W = 0$, and $2A = 0$). $I'(S)$, the integrated intensity per unit width, is related to $I(S)$ through the following equation:

$$I'(S) = \frac{1}{2W} \int_{S-W}^{S+W} \left(\frac{1}{2A} \int_{S'-A}^{S'+A} I(S'')\, dS'' \right) dS', \tag{5}$$

where S', S'' are simply transient variables for integration.

In our case, $2W = 22$ μ and $2A = 14$ μ. Through Eq. (5), it is found that for S between 0.005 and 0.14 cm, the difference between $I'(S)$ and $I(S)$ is small [$I'(S)$ is 4% greater than $I(S)$ for $S = 0.005$ cm and there are trivial differences at greater distances], and also found that the effect of the interaction is to move S_0 into the geometric shadow of the surface by less than 0.00013 cm from the position it would be if the interaction is "turned off." The discussion here is based on the

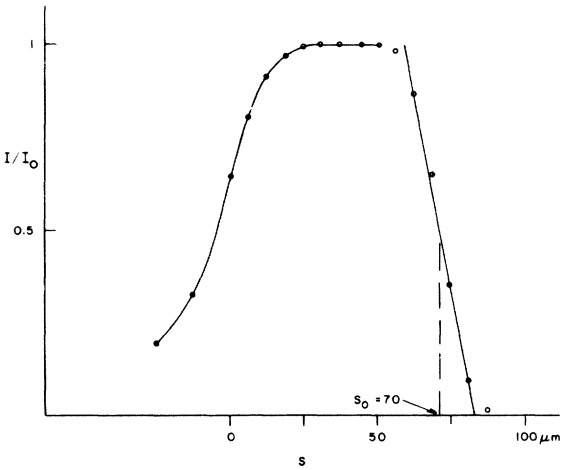

FIG. 2. Typical measured intensity drop showing the determination of S_0.

TABLE I. Comparison between the theoretical beam profiles calculated by the numerical method and by the 11-term expansion. Here, the case $\beta = 1.4\times 10^{-23}$, $r_0 = 5$ cm is shown.

S(cm)	$(I/I_0)_1$ [a]	$(I/I_0)_2$ [b]	Δ [c]
0.0203	8.71×10^{-5}	8.70×10^{-5}	
0.0398	2.28×10^{-5}	2.29×10^{-5}	
0.0627	6.71×10^{-6}	6.77×10^{-6}	+0.8%
0.0832	2.49×10^{-6}	2.57×10^{-6}	+3.2%
0.1036	9.62×10^{-7}	10.19×10^{-7}	+5.9%

[a] Relative intensity calculated by the numerical method.
[b] Relative intensity calculated by 11-term S expansion.
[c] $\Delta = [(I/I_0)_2 - (I/I_0)_1]/(I/I_0)_1$.

interaction of the form $-K/r^3$, where K is the value determined in the subsequent experiment.

THEORETICAL BEAM PROFILE

Classical orbit theory is used to find the trajectory of a particle that approaches the cylinder of radius r_0 with an impact parameter a, and subject to a potential of the form $V = -K/R^3$, where R is the distance between the particle and the surface, and K is a constant. This trajectory depends on the constant $\beta = K/E$, where E is the kinetic energy of the particle. In a plane at a distance l_2 from the cylinder, the deflection S of the particle is given by

$$S = l_2(2\varphi_{\max} - \pi), \tag{6}$$

where we have

$$\varphi_{\max} = \int_{r_m}^{\infty} \frac{dr}{r[F(r)]^{1/2}}$$

and

$$F(r) = \frac{r^2}{(r_0+a)^2} + \frac{\beta r^2}{(r_0+a)(r-r_0)^3} - 1,$$

where r is the distance of the particle from the cylinder axis.

The minimum distance r_m of the orbit from the cylinder axis is found from $F(r_m) = 0$. We write $r_m = r_0 + \lambda_m$, where λ_m is the distance of closest approach to the cylinder surface. Then we find

$$\lambda_m^3(a - \lambda_m) = \tfrac{1}{2}\beta r_0 \tag{7}$$

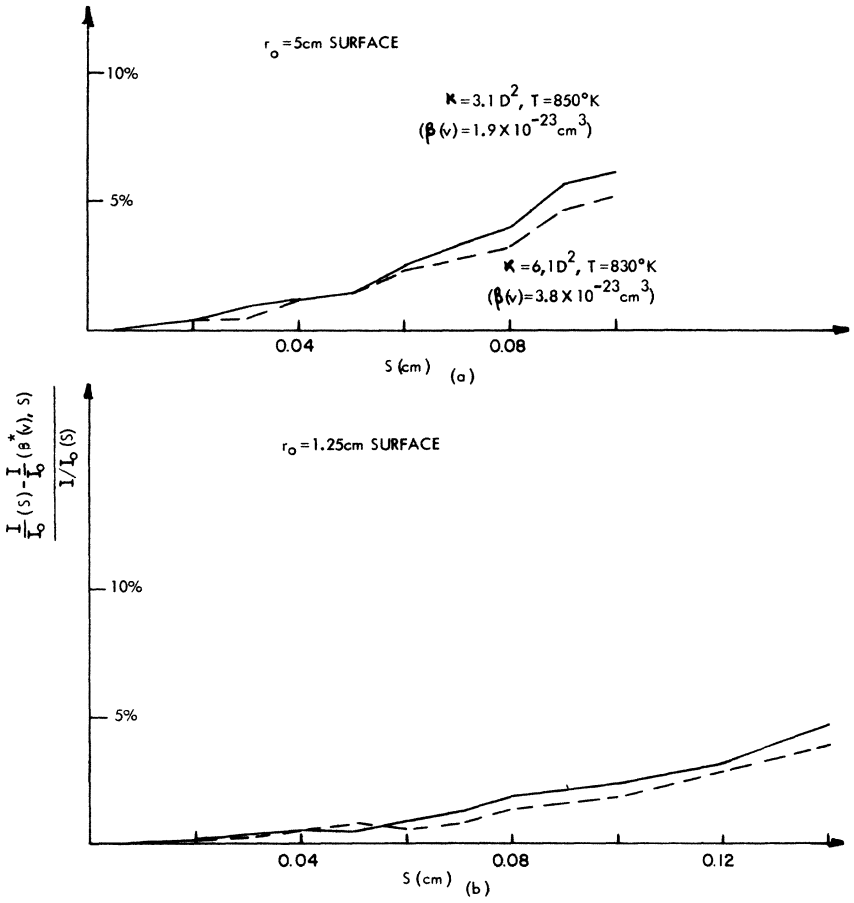

FIG. 3. Effect of velocity distribution on a beam profile is shown by comparing the ideal beam profile $I(\bar{\beta},S)/I_0$ to the profile $I(S)/I_0$ calculated by Eq. (16).

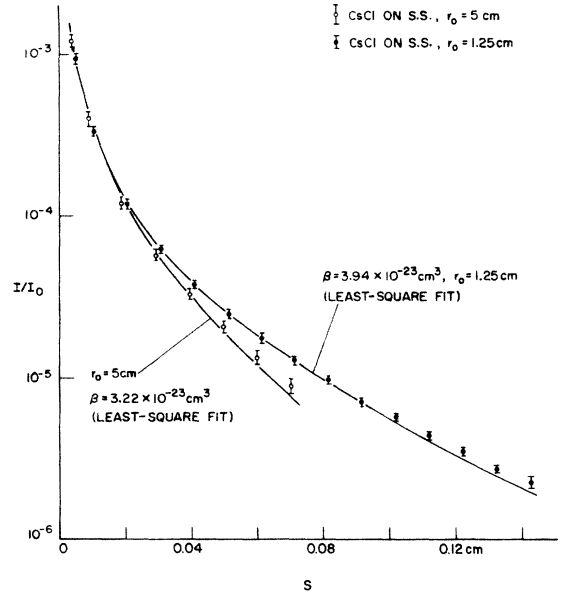

FIG. 4. Observed profiles of a CsCl beam deflected by stainless-steel surfaces are compared to their respective least-squares adjusted theoretical profiles.

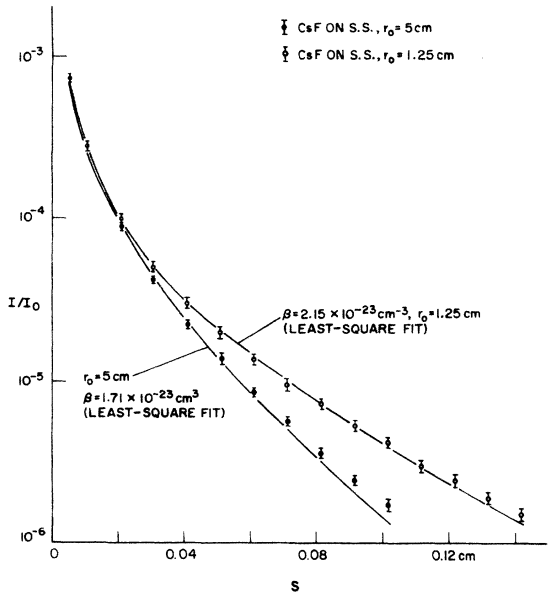

FIG. 5. Observed profiles of a CsF beam deflected by stainless-steel surfaces are compared to their respective least-squares adjusted theoretical profiles.

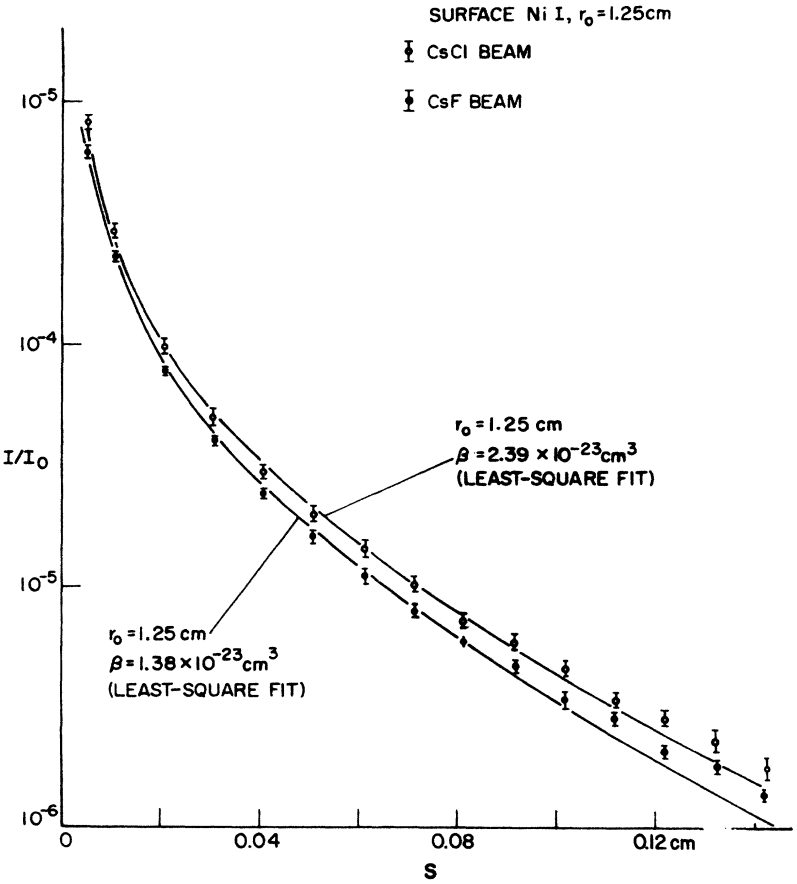

FIG. 6. Observed profiles of a CsCl and CsF beam. The deflector is the electroless nickel surface Ni I.

to a very high degree of approximation, since we know a, $\lambda_m \ll r_0$.

For the purpose of calculation λ_m is used as the independent variable. It can be shown that Eq. (7) has a real solution λ_m only if the impact parameter a is greater than a_1, where a_1 is given by

$$a_1 = \tfrac{4}{3}(\tfrac{3}{2}\beta r_0)^{1/4}. \tag{8}$$

Particles with impact parameters less than a_1 are captured by the surface and thus do not reach the detector. The minimum value of λ_m is given by

$$\lambda_{m\,\min} = \tfrac{3}{4}a_1. \tag{9}$$

The intensity per unit width, I, in the detector plane relative to the full beam intensity per unit width, I_0, is expressed by

$$\frac{I}{I_0} = \frac{l/l_1}{l/l_1 - dS/da}, \tag{10}$$

where l_1 is the distance between the slit S_1 and the surface, and $l = l_1 + l_2$.

It is not possible to integrate the expression for $\varphi_{\max}$ directly in terms of elementary functions. An expression for S in terms of an infinite series was derived,[6] and the first five terms are

$$S = \sum_{n=1} S_n = \frac{15\pi l_2 \delta}{8(2r_0\lambda_m)^{1/2}} \times[1 + 1.192(\delta/\lambda_m) + 2.285(\delta/\lambda_m)^2 + 5.054(\delta/\lambda_m)^3 + 12.02(\delta/\lambda_m)^4 + \cdots], \tag{11}$$

where

$$\delta = a - \lambda_m = \beta r_0/2\lambda_m^3.$$

Using this expansion, Eq. (10) can be expressed by

$$\frac{I}{I_0} = \frac{4.175(\lambda_m - 3\delta)}{7S + 8\sum_{n=2}(n-1)S_n}. \tag{12}$$

In practice, S is expanded to eleven terms. The rate or convergence of this series is slow for cases involving relatively small β and large S. For example, we choose $\beta = 1.4\times10^{-23}$ cm^3, $r_0 = 5$ cm and $\lambda_m = 333$ Å, and lead to $S = 0.101$ cm by the eleven-term expansion. In calculating this S we find that 6.5% of its value is contributed by terms 7–11. When we calculate I/I_0 at this S, we

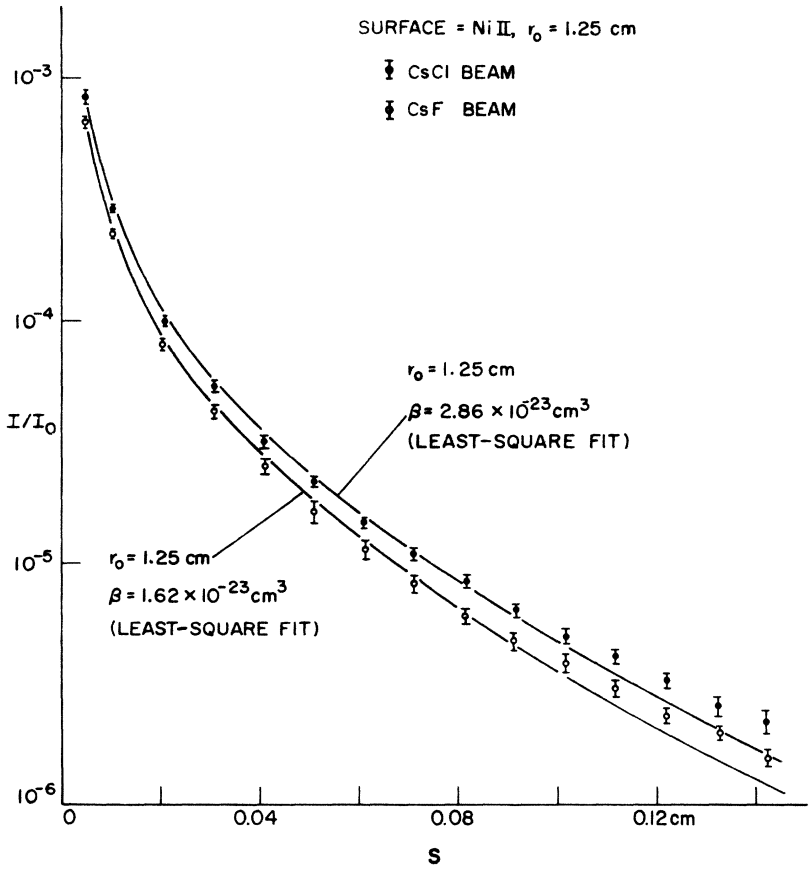

FIG. 7. Observed profiles of a CsCl and CsF beam. The deflector is the surface Ni II.

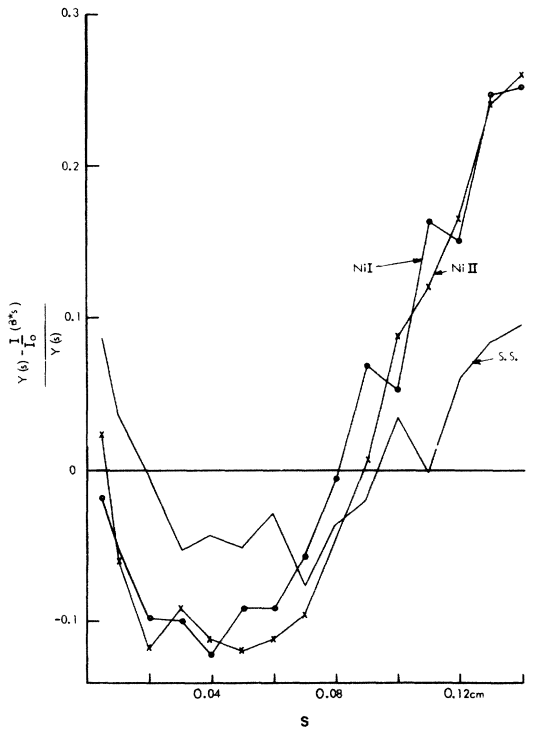

FIG. 8. Systematic deviation of a measured profile $Y(S)$ from the least-squares adjusted theoretical profile $I(\beta,S)/I_0$ is demonstrated by the fractional deviation function plotted against the deflection distance S. The profiles of a CsF beam deflected by a stainless-steel surface and two electroless nickel surfaces are selected for illustration.

find that 32% is contributed by terms 7–11.

To check the accuracy of the beam profile calculated by the eleven-term expansion of S, the integration involved in Eq. (6) is performed numerically. The difference between φ_{max} and $\frac{1}{2}\pi$ is extremely small. In order to evaluate S, φ_{max} has to be known precisely to many significant figures. Alternatively, the following identity can be used to express $\frac{1}{2}\pi$ so that the subtraction is performed within the integrand. We use

$$\frac{\pi}{2} = \int_{r_m}^{\infty} \frac{dr}{r(r^2/r_m^2 - 1)^{1/2}} . \tag{13}$$

The change of the variable of integration, $R = r_m/r$, in Eqs. (6) and (13) leads to

$$S = 2l_2\left(\int_0^1 \frac{dR}{[H(R)]^{1/2}} - \int_0^1 \frac{dR}{(1-R^2)^{1/2}} \right), \tag{14}$$

where $H(R) = R^2F(r_m/R)$.

As R approaches 1, $H(R)^{-1/2}$ approaches $(1-R^2)^{-1/2}$. Consequently, Eq. (14) can be conveniently integrated by means of the Gauss-Mehler quadrature formula[10]

$$\int_{-1}^{1} f(x)(1-x^2)^{-1/2}\,dx = \frac{\pi}{N}\sum_{\kappa=1}^{N} f(\cos\alpha_\kappa), \tag{15}$$

where

$$\alpha_\kappa = (2\kappa - 1)\pi/2N.$$

For N even,

$$S = 2l_2\frac{\pi}{N}\sum_{\kappa=1}^{N/2}[G(R_\kappa) - 1], \tag{16}$$

with

$$G(R_\kappa) = \left(\frac{1-R_\kappa^2}{H(R_\kappa)}\right)^{1/2},$$

$$R_\kappa = \cos\left(\frac{2\kappa-1}{2N}\right)\pi .$$

The same numerical method can be used to evaluate I/I_0, since

$$\frac{I}{I_0} = \frac{l/l_1}{l/l_1 - dS/da} \tag{17}$$

and

$$\frac{dS}{da} = -\frac{1}{2}\int_0^1 \frac{dH/da}{H(R)^{3/2}}\,dR.$$

The accuracy of the numerical integrations is checked by comparison with integrations using larger numbers of steps, i.e., larger N in Eq. (15). The calculated values of S and I/I_0 remains essentially stable when N increases from 10 000 to 30 000. With $N = 10\,000$, we calculated $I(S)/I_0$ for $\beta = 1.4\times10^{-23}$ cm^3 and $r_0 = 5$ cm, and the comparison with the eleven-term expansion result as shown in Table I. One notices that at larger S the integrated I/I_0 is lower than I/I_0 by the expansion

TABLE II. Observed values of β (in units of 10^{-23} cm^3).

	Stainless-steel surface ($r_0 = 5$ cm)	Stainless-steel surface ($r_0 = 1.25$ cm)	Ni I surface ($r_0 = 1.25$ cm)	Ni II surface ($r_0 = 1.25$ cm)	Theoretical β [a]
CsF	1.71 ± 6%	2.15 ± 4%	1.38 ± 7.9%	1.62 ± 7.8%	3.12
CsCl	3.22 ± 8%	3.94 ± 3.7%	2.39 ± 6.3%	2.86 ± 5.6%	5.75
$\frac{\beta(\text{CsF})}{\beta(\text{CsCl})}$	0.53	0.55	0.58	0.57	0.54

[a] β is calculated based on the classical dipole and image-dipole models.

TABLE III. Observed values of K (in units of $D^2 = 10^{-36}$ esu).

	Stainless-steel surface ($r_0 = 5$ cm)	Stainless-steel surface ($r_0 = 1.25$ cm)	Ni I surface ($r_0 = 1.25$ cm)	Ni II surface ($r_0 = 1.25$ cm)	Theoretical K [a]
CsF	2.81 ± 7%	3.53 ± 5%	2.27 ± 9%	2.66 ± 9%	5.16
CsCl	5.17 ± 9%	6.32 ± 5%	3.83 ± 7%	4.59 ± 7%	9.2
$\frac{K(\text{CsF})}{K(\text{CsCl})}$	0.55	0.56	0.59	0.58	0.56

[a] K is calculated based on the dipole and image-dipole models.

method. Later, we will show that the experimental beam profiles apparently deviate systematically from the theoretical curves calculated by the expansion method. This deviation is increased if the more accurate theoretical beam profiles are used.

We have, thus far, considered the beam profile of a monoenergetic beam. For a beam of particles of mass M effusing from an oven at a temperature T, the velocity distribution of the particles in the beam is described by

$$f(v)\,dv = 2(v/\alpha)^3 e^{-(v/\alpha)^2} d(v/\alpha), \tag{18}$$

where $\alpha = (2kT/m)^{1/2}$ (k = Boltzmann's constant). Thus, the observed beam profile is

$$I(S) = \int_{v=0}^{\infty} I[\beta(v), S] f(v)\,dv. \tag{19}$$

With an instantaneous interaction approximation, it was shown[6] that $I(S)$ is very nearly $I[\beta(\bar{v}), S]$, where $\bar{v} = 1.2\alpha$, and $\beta(\bar{v}) = K/1.4kT$. We will examine here how well $I[\beta(\bar{v}), S]$ approximates the actual profile. After the transformation $X = (v/\alpha)^2 = K/kT\beta$, Eq. (19) is integrated by means of the Gauss-Laguerre quadrature formula[11]

$$\int_0^{\infty} X e^{-X} f(X)\,dX = \sum_{i=1}^{N} A_i f(X_i), \tag{20}$$

where the values of A_i and X_i can be found in the table in Ref. 11. Thus, we have

$$I(S) = \sum_{i=1}^{N} A_i I(K/kTX_i, S). \tag{21}$$

In practice, formulas with $N = 12$ are used and the result agrees well with that by $N = 16$. The deviations of the monoenergetic beam profile $I(\beta(\bar{v}), S)$ from the profile of the full velocity distribution $I(S)$ are demonstrated in Fig. 3 by plotting $[I(S) - I(\beta(\bar{v}), S)]/I(S)$ against S.

Theoretical beam profiles corrected for the velocity distribution are used in analyzing data.

RESULTS

The measured beam profiles cannot be fitted precisely with the theoretical profiles based on an assumed inverse cube interaction potential. The least-squares adjustment of the observed profile to a theoretical profile is made, and in Figs. 4–7 the observed profiles are shown together with the least-squares fitted theoretical profiles. With the method of the least-squares adjustment used here[12] the quantity being minimized is

$$Q = \sum_i [I(\beta, S_i)/I_0 - Y(S_i)]^2/\sigma_i^2, \tag{22}$$

where $Y(S_i)$ is the observed intensity at the deflection distance S_i, $I(\beta, S_i)/I_0$ is the calculated value, and σ_i is the standard deviation in $Y(S_i)$.

The deviation between observed and calculated

TABLE IV. Experimental parameters β', β, or β'' resulting from the least-squares adjustment of observed beam profiles to theoretical profiles based on an r^{-2}, r^{-3}, or r^{-4} potential, respectively.

	CsF on stainless steel ($r_0 = 5$ cm)	CsF on stainless steel ($r_0 = 1.25$ cm)
Least-squares determined β' $[V'(r) = -\kappa'/r^2,\ \beta' = \kappa'/E]$	$(2.41 \times 10^{-18}) \pm 12\%$ cm^2	$(3.82 \times 10^{-18}) \pm 8\%$ cm^2
Least-squares determined β $[V(r) = -\kappa/r^3,\ \beta = \kappa/E]$	$(1.71 \times 10^{-23}) \pm 4\%$ cm^3	$(2.15 \times 10^{-23}) \pm 6\%$ cm^3
Least-squares determined β'' $[V''(r) = -\kappa''/r^4,\ \beta'' = \kappa''/E]$	$(1.92 \times 10^{-28}) \pm 4\%$ cm^4	$(1.89 \times 10^{-28}) \pm 9\%$ cm^4

values are systematic and qualitatively the same in all cases. In spite of this small deviation, the least-squares-determined β does give a pretty good representation of the phenomenon as described in elementary theory.

The functional deviation just stated is clearly illustrated by the fraction of deviation as the function of the deflection distance S, that is,

$$f(S)=[Y(S)-I(\beta,S)]/Y(S), \tag{23}$$

where $Y(S)$ is the observed intensity and $I(\beta,S)$ is the calculated value with least-squares-determined β. This function is shown in Fig. 8 for three cases. The deviation is qualitatively the same for all cases, namely, the observed intensities at large deflection distances are larger than the calculated values, and the contour of the function $f(s)$ is U shaped.

When the systematic deviation is ignored, approximate values of β are derived through the least-squares adjustment and listed in Table II. The interaction constant K is calculated from β by the relation $K=(1.4kT)\beta$ and listed in Table III. The term T, the evaporation temperature of the beam, is 830°K for CsCl and 850°K for CsF. Each of these constants K is found to be a fraction (between 0.42 and 0.68) of the value predicted by the dipole and image dipole model. The theoretical values used in Table III are the lower limit expected for a CsCl and CsF molecule interacting with an ideal conducting surface. The low experimental values of the interaction constants may indicate the imperfection of stainless steel and electroless nickel as conductors. Because of the complexity of these materials, we are not capable of using the existing theories to calculate the interaction constants for such surfaces.

In spite of the disagreement between the observed and the calculated constants based on the dipole and image-dipole model, it is interesting to note that, for an identical surface, the observed ratio of the interaction constant for CsF to that for CsCl agrees well with the ratio predicted by the elementary model.

The observed beam profiles and therefore the derived interaction constants are different for two otherwise identical electroless nickel surfaces for both CsCl and CsF beams by about 17%.

The measurements have been repeated five times at each of four different locations on the 5-cm radius stainless-steel surface (each is 90° arc length from the next one). The interaction constants for each location are least-squares determined, and found to be respectively 2.64, 2.78, 2.94, and 2.91 in units of D^2 (about a 10% difference between the maximum and minimum values).

For an identical molecular beam, the observed interaction constant is larger for a stainless-steel surface than for either of the electroless nickel surfaces. The discrepancy in interaction constants between surfaces of two different materials is more than between surfaces of the same material.

There is a discrepancy in interaction constants derived from two stainless-steel surfaces of different radii and with either a CsF or CsCl beam, the observed interaction constant for a 1.25-cm radius surface being larger than for a 5-cm surface.

The observed beam profiles of a CsF beam deflected by stainless-steel surfaces of radii 5 cm and 1.25 cm are also least-squares adjusted to a theoretical profile based on an assumed potential $V'(r)=-K'/R^2$ or $V''(r)=-K''/R^4$, where R is the separation between the particle and the surface; K' and K'' are constants. In Table IV, the least-squares-determined parameters β' and β'' are listed, with $\beta'=K'/E$ and $\beta''=K''/E$, where E is the kinetic energy of the particle. The fractional deviation function $f(S)$ defined earlier is again used to demonstrate how the observed profiles compared with calculated profiles based on r^{-2}, r^{-3}, or r^{-4} potentials, and this function $f(S)$ is plotted in Fig. 9 for each of the three potentials.

We find that it is reasonable to prefer an r^{-3} potential to an r^{-2} potential, based on the following observations. (i) As a function, the observed beam profile deviates more from the theoretical profile based on an r^{-2} potential than from that based on an r^{-3} potential. (ii) In comparison with

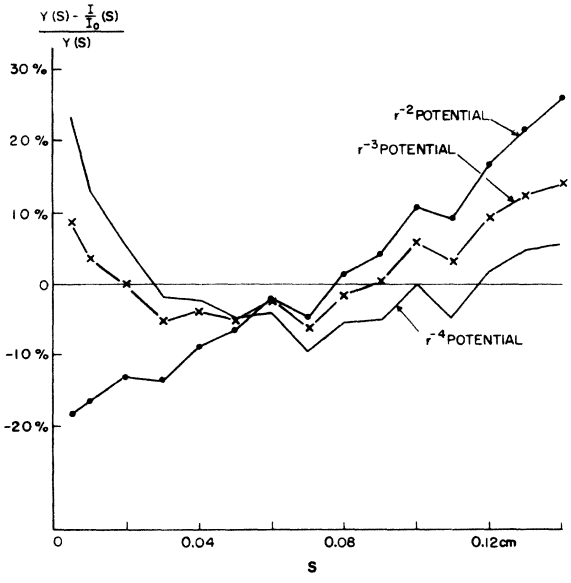

FIG. 9. Deviations of the least-squares fitted theoretical profiles $I(S)/I_0$ based on an r^{-2}, r^{-3}, or r^{-4} potential from the observed beam profiles of CsF deflected by a stainless-steel surface with 1.25-cm radius.

an r^{-2} potential, the observed beam profiles involving two surfaces of different radii (5 cm and 1.25 cm) give two β' with large discrepancies $\{[\beta'(1.25\text{ cm}) - \beta'(5\text{ cm})]/\beta'(5\text{ cm}) = 58\%\}$, whereas $[\beta(1.25\text{ cm}) - \beta(5\text{ cm})]/\beta(5\text{ cm}) = 26\%$ when β is associated with an r^{-3} potential.

However, we find no mathematical reason to prefer an r^{-3} potential to an r^{-4} potential. In fact, the parameters derived from the beam profiles of surfaces with 5-cm and 1.25-cm radii are in better agreement if the assumed potential is r^{-4} than if the assumed potential is r^{-3}. {We have $[\beta(1.25\text{ cm}) - \beta(5\text{ cm})]/\beta(5\text{ cm}) = 26\%$, whereas $[\beta''(1.25\text{ cm}) - \beta''(5\text{ cm})]/\beta''(5\text{ cm})$ is trivial.} Nevertheless, we have accepted an r^{-3} potential instead of an r^{-4} potential solely on the grounds that an r^{-3} potential has a theoretical basis and the observed interaction constants agree with predicted values, based on the simplest model, within a factor of 2.

---

*Work supported by the Army Research Office, Durham, under Grant No. DA-ARO-D-31-124-G-972, and the Joint Service Electronics Program under Contract No. DAAB07-69-0383.

†Present address: Surface Chemistry Section, National Bureau of Standards, Washington, D. C. 20234.

‡Present address: Metropolitan Transportation Authority, N. Y., N. Y. 10019.

§Present address: Department of Physics, Univ. of Texas, Dallas, Texas 75230.

[1]J. E. Lennard-Jones, Trans. Faraday Soc. 28, 333 (1932).

[2]A. Shih, thesis (Columbia University, 1972) (unpublished), p. 141.

[3]J. Bardeen, Phys. Rev. 58, 727 (1940).

[4]C. Mavroyannis, Mol. Phys. 6, 593 (1963).

[5]H. B. G. Casimir and D. Polder, Phys. Rev. 73, 360 (1948).

[6]D. Raskin and P. Kusch, Phys. Rev. 179, 712 (1969).

[7]D. Lando and L. J. Slutsky, Phys. Rev. B 2, 2863 (1970).

[8]P. M. Waters, Phys. Rev. 111, 1053 (1958).

[9]J. W. Frazer, R. P. Burns, and G. W. Barton, Rev. Sci. Instrum. 30, 370 (1959).

[10]V. I. Krylov, *Approximate Calculation of Integrals* (MacMillan, New York, 1962), pp. 115, 130.

[11]P. Rabinowitz and G. Weiss, *Mathematical Tables and Other Aids to Computation* (National Research Council, Washington, D. C., 1959), Vol. 13, pp. 285–293.

[12]W. E. Wentworth, J. Chem. Education 42, 2 (1965).